

A catalogue sample of low mass galaxies observed in X-rays with central candidate black holes

A. A. Nucita, L. Manni, F. De Paolis, M. Giordano, and G. Ingrosso

Department of Mathematics and Physics “E. De Giorgi”, University of Salento, Via per Arnesano, CP 193, I-73100, Lecce, Italy

INFN, Sez. di Lecce, Via per Arnesano, CP 193, I-73100, Lecce, Italy

Corresponding author:

nucita@le.infn.it

ABSTRACT

We present a sample of X-ray selected candidate black holes in 51 low mass galaxies with $z \leq 0.055$ and mass up to $10^{10} M_{\odot}$ obtained by cross-correlating the NASA-SLOAN Atlas with the 3XMM catalogue. We have also searched in the available catalogues for radio counterparts of the black hole candidates and find that 19 of the previously selected sources have also a radio counterpart. Our results show that about 37% of the galaxies of our sample host an X-ray source (associated to a radio counterpart) spatially coincident with the galaxy center, in agreement with other recent works. For these *nuclear* sources, the X-ray/radio fundamental plane relation allows one to estimate the mass of the (central) candidate black holes which results to be in the range $10^4 - 2 \times 10^8 M_{\odot}$ (with median value of $\approx 3 \times 10^7 M_{\odot}$ and eight candidates having mass below $10^7 M_{\odot}$). This result, while suggesting that X-ray emitting black holes in low-mass galaxies may have had a key role in the evolution of such systems, makes even more urgent to explain how such massive objects formed in galaxies. Of course, dedicated follow-up observations both in the X-ray and radio bands, as well as in the optical, are necessary in order to confirm our results.

Subject headings: X-rays: massive black holes

1. Introduction

Low mass galaxies with stellar mass less than $\approx 1 \times 10^{10} M_{\odot}$ are faint galaxies, particularly hard to be detected and studied. The objects with mass below $\approx 5 \times 10^9 M_{\odot}$ are usually classified as isolated or satellite dwarf galaxies being this value the visible mass of the Large Magellanic Cloud (Gyuk et al. 2000; Conroy & Bullock 2015).

Low mass galaxies span all the possible shape classification from spirals to ellipticals through irregular objects¹.

¹ In this context, dwarf spheroidal galaxies are a sub-class of low mass galaxies with stellar mass in the range $10^3 - 10^7 M_{\odot}$ (Martin et al. 2008) particularly interesting since they show large mass-to-light ratios which make them to be dominated by dark matter (Mateo 1997). The interest in dwarf galaxies is rapidly growing (see, e.g., McConnachie 2012) both for stellar populations studies (Amorisco & Evans 2012; Maccarone et al. 2005) and searches for central IMBHs (see e.g., Reines et al. 2013, Nucita et al. 2013a,

It is known that massive black holes² are hosted in the nuclei of almost every galaxy characterized by a central bulge (Kormendy & Ho 2013). In these cases, black holes reveal themselves via stellar and gas kinematic in close targets or, in distant active galactic nuclei, by mean of the emitted radiation. By extrapolating the fundamental $M_{BH} - M_{Bulge}$ relation (Magorrian et al. 1998, for the super massive BH case

Nucita et al. 2013b, Manni et al. 2015).

²The paradigm of the existence of massive black holes in the center of almost all galaxies comes from indirect observations at several wavelengths. In the next future, the Event Horizon Telescope (which is based on techniques of Very Long Baseline Interferometry -VLBI- see, e.g., Ricarte & Dexter 2015) will achieve the μ -arcseconds angular resolution necessary to resolve the shadows of massive black holes at least in nearby galaxies (see, e.g., Falcke, Melia, & Agol 2000 for the Sgr A* case). In these cases, the shape of such shadows will allow one not only to have the first direct evidence of the existence of such objects but also to get an estimate of their mass, spin and charge parameters (see, e.g., Nucita et al. 2007; De Paolis et al. 2011; Zakharov et al. 2012).

but see also Reines & Volonteri 2015) down to the typical mass of low mass galaxies, one realizes that intermediate mass black holes (IMBHs) may also be found in such stellar systems. Their number density and characteristics is, in turn, of crucial importance to get information about the black hole seed population in the early Universe (Volonteri 2010; Natarajan 2014) and about their contribution in re-ionizing the hydrogen at high red-shift via the X -ray emission (Volonteri & Gnedin 2009). Furthermore, searching for the high energy emission expected from these objects and applying the fundamental plane relation at radio and X -ray wavelengths (see Merloni et al. 2003) as recently done by several authors (see e.g., Reines et al. 2013, Nucita et al. 2013a, Nucita et al. 2013b) allows one to infer the mass of the compact object (if any).

Recently, Lemons et al. (2015) cross-matched a sample of 44000 dwarfs (provided by the NASA-Sloan Atlas³) with mass within $3 \times 10^9 M_{\odot}$ and at a redshift as large as $z < 0.055$ with the Chandra Source Catalogue (Evans et al. 2010) finding a heterogeneous sample of 19 galaxies with a total of 43 point-like X -ray sources with hard spectra and 2 – 10 keV luminosities between $10^{37} \text{ erg s}^{-1}$ and $10^{40} \text{ erg s}^{-1}$, i.e. in the typical range of power emitted by stellar-mass X -ray binaries and massive black holes accreting at low Eddington rate. Of these sources, the author set an upper limit of 53% on the fraction of galaxies in the sample having a hard X -ray source located in the optical nucleus, although this region is generally poorly constrained for most of the dwarfs. Furthermore, Nucita et al. (2013a,b); Manni et al. (2015) have focused their attention on a sample of five dwarf spheroidal Milky Way satellites (i.e., Fornax, Ursa Minor, Draco, Leo I, and Ursa Major II) since, due their proximity and the lack of overcrowded environment, allows one to characterize (on statistical basis) the nature of the identified X -ray sources. In particular, it were found hints of the existence of central massive black holes in $\approx 40\%$ of the cases, but it was also derived a small contamination due to a few local stellar-mass X -ray binaries so that follow-up observations are required to disentangle between the stellar-mass X -ray binary and active galactic nucleus with an accreting black hole scenarios.

In this paper, we search for the signatures of massive black holes in low mass galaxies by using archival data from the XMM -Newton satellite. In spite of its low angular resolution ($\approx 6''$, primarily due to the

³<http://www.nsatlas.org>.

point spread function - PSF - of the mirror modules, see e.g. *XMM-Newton Users Handbook* 2015; *XRPS User's Manual* 2008), XMM -Newton is particularly useful for studying faint objects (as the low accreting/emitting massive black holes targets of this study) thanks to its large effective area (Jansen et al. 2001). We cross-correlated the NASA-Sloan Atlas with the 3XMM-DR5 catalogue (Rosen et al. 2016), which is five times the current size of the Chandra source catalogue (Evans et al. 2010) producing a starting galaxy sample. For each target, we retrieved and analyzed the original XMM -Newton data products (ODFs), produced images in the 0.2 – 12 keV energy band and accumulated spectra for each of the matched sources.

Our catalogue (hereafter GiX, i.e. galaxies in X -rays) resulted in 51 galaxies detected by using the XMM -Newton satellite. The corresponding masses turn out to span between about 1.5×10^8 and $10^{10} M_{\odot}$, with $5.4 \times 10^9 M_{\odot}$ as the median value. A further cross correlation of GiX with FIRST⁴ (the VLA FIRST Survey: Faint Images of the Radio Sky at Twenty cm), NVSS⁵ (the NRAO VLA Sky Survey), and the catalogue of X -ray selected star-forming galaxies within the *Chandra Deep Field-South* by Rosa-Gonzalez et al. (2007) (hereafter, RG2007) resulted in 19 radio counterparts allowing us to use the fundamental plane relation (see Merloni et al. 2003) and infer the black hole mass.

This paper is organized as follows. In Sect. 2 our main galaxy sample is outlined. In Sect. 3 we give details on the data analysis of the XMM -Newton data. In Sect. 4 we present the cross-correlation among the GiX and FIRST, NVSS and RG2007 catalogues and use the fundamental plane relation to estimate the black hole masses. Finally, in Sect. 5, we address our results.

2. The GiX sample

The NASA-Sloan Atlas is a catalogue of local galaxies (145155 objects up to redshift $z \approx 0.055$) based on reanalysis of optical and ultraviolet observations conducted for the SDSS and Galaxy Evolution Explorer (GALEX). Querying the catalogue results in various galaxy parameters as the distance and mass estimate based on the *kcorrect* code of

⁴The FIRST catalogue is available at <http://sundog.stsci.edu/>.

⁵The NVSS catalogue is available at <http://www.cv.nrao.edu/nvss/>.

Blanton & Roweis (2007). In particular, the mass of each galaxy is given in units of $M_{\odot}h^{-2}$ and we adopt $h = 0.73$ (see also the next Section).

We decided to consider galaxies with masses $\lesssim 10^{10} M_{\odot}$, i.e. a factor 3.3 larger than what assumed in Lemons et al. (2015) (but see also Mezcua et al. 2016; Pardo et al. 2016). Hence, we selected 82977 galaxies from the NASA-Sloan Atlas, a number which reduces to 44594 objects with mass up to $3 \times 10^9 M_{\odot}$, consistent with Lemons et al. (2015). Note that under these assumptions, our selected objects would not be properly classified as dwarf galaxies.

We do not set a lower limit for the stellar mass because the parental Sloan catalogue contains objects with mass greater than $1 \times 10^7 M_{\odot}$ due to the $r < 17$ spectroscopic apparent magnitude limit of SDSS. As in Reines et al. (2013), we further put some constraints on the spectroscopic values of the SDSS sample. In particular, we selected only sources with $EW > 1 \text{ \AA}$ and $S/N \geq 3$ for $H\alpha$, $[NII]$ and $[OIII]$, whereas $S/N \geq 2$ for $H\beta$. Finally, our parent low mass galaxy sample is constituted by 47959 sources⁶.

We then searched for galaxy counterparts in X-rays in the recent fifth release of the 3XMM catalogue (3XMM-DR5, Rosen et al. 2016), the largest X-ray source catalogue ever produced. For each detected sources, one has the fluxes and count rates in 7 X-ray energy bands, the total 0.2 – 12 keV band counts, and four hardness ratios, as well as the associated celestial coordinates and a measure of the detection quality (controlled via the the detection summary flag *SUM_FLAG*). We only considered sources characterized by a detection quality of 0 (good sources) or 1 (if at least one of the warning flags - indicating low detector coverage, proximity to other sources, within extended emission, and/or near bright corner of CCD - was activated, but no possible-spurious-detection flags were on). We verified that the interesting sources of our sample have a maximum detection likelihood value (defined as $-\ln(P)$, where P is the probability of the detection occurring by chance) larger than $\simeq 6.7$. In the association procedure, a galaxy of our sample was considered cross-matched with a corresponding source in the 3XMM-DR5 catalogue if their distance was less or equal than $3''$.

For each of the interesting source, we retrieved the

⁶ When we restrict the upper value of the galaxy mass to $3 \times 10^9 M_{\odot}$ we find 25974 objects which is exactly the number found by Reines et al. (2013) when adopting the same selection criteria.

XMM-Newton raw data files (ODF) and produced X-ray images in the 0.2 – 12 keV band (see next Section for details on the data reduction pipeline). We visually inspected the images in order to eliminate faked sources. Hence, our final GiX catalogue is constituted by 51 targets with 40 sources characterized by 0 detection quality flag, and 11 with this flag set to 1. In Table 1, we give a sequential number, the XMM-Newton OBSID, the NASA-Sloan Atlas ID, the common galaxy name, the target coordinates (J2000 RA and DEC in degrees), the distance (in arcseconds) between the galaxy center and the cross-matched X-ray source, the galaxy mass according to the NASA-Sloan Atlas, the *SUM_FLAG* (labeled as SF) value characterizing the quality of the X-ray observation, and the relative net counts along with the corresponding error, respectively. It is worth noting that all of our sources (except the source #36) seem to be point-like as suggested by the extent parameter derived by the SAS task *emldetect* and used when compiling the 3XMM catalogue. In the case of the aforementioned source #36, the associate extension is $\simeq 7.4''$ prompting to a non point-like origin and possibly related to a non resolved source group. In this context, the black hole mass for source #36 estimated via the X-ray/radio fundamental plane (see next) has to be considered as a lower limit.

3. X-ray data analysis

In this paper, we used an ab-initio procedure in order to get estimates of the source fluxes in the 0.2 – 12 keV and 2 – 10 keV bands and not relied blindly on the data available on the 3XMM-DR5 catalogue. The observation data files (ODFs) were processed using the XMM-Science Analysis System (SAS version 14.0.0) together with the most updated calibration constituent files.

The event lists for the three EPIC cameras were obtained by using the standard *emchain* and *epchain* tools following standard procedures for the screening part (XRPS User’s Manual 2008). In particular, we rejected time intervals characterized by high levels of background activity. In this respect, we constructed light curves in the energy range 10 – 15 keV with a given bin size, evaluated the mean and the standard deviation σ of the time series and cut the time intervals with a number of counts per bin larger than 3σ . We iterated the whole procedure until the number of counts per bin is constant⁷. In presence of observations af-

⁷ A similar approach giving comparable results is described in

ected by large flares, we used a more restrictive cut by simply requiring to have a threshold of 0.4 counts s^{-1} and 0.35 counts s^{-1} for the pn and MOS cameras, respectively.

We produced images in the 0.2–12 keV band for the three cameras visually searching for point-like sources at the nominal coordinates of the galaxies in our sample. We then extracted the source spectra (with extraction radius in the range $\simeq 25'' - 50''$) by applying the filter expressions `#XMMEA_EM` (for MOS) and `#XMMEA_EP` (for pn) and added the expression `FLAG == 0` in order to reject events close to CCD gaps or bad pixels. We also accounted for all the valid patterns (`PATTERN` in [0:12]) for the two MOS cameras while restricted the analysis to single and double events (`PATTERN` in [0:4]) for pn. When possible, the related background spectra were extracted on an annulus surrounding the target source or on a circle close to it.

The EPIC source (background-corrected) spectra were re-binned to have at least 25 counts per energy bin for bright source, while we relaxed this requirement and used 15 counts per bin for fainter targets. Further, the spectra (as well as the ancillary files and response matrices) were imported and used in XSPEC (version 12.9.0) to manage the spectral analysis and for fitting purposes.

For each target we inspected the spectrum and fit it with a model consisting in an absorbed power-law (model A in Table 2) with hydrogen column density fixed to the value given (fifth column) by the *NH Tool*⁸ (which is based on Kalberla et al. 2005) towards the source coordinates. In a few cases, the fit procedure converged towards meaningless values of the power-law index, thus forcing us to fix it to the value $\Gamma = 1.7$ (in accordance to default value used in the 3XMM catalogue) thus leaving the power-law normalization as the single free fitting parameter⁹. The XSPEC implementation of the model is `const*phabs*powerlaw`, with the `const` accounting for cross-calibration issues among the *XMM-Newton* instruments. For some cases, we fixed both the hydrogen column density and the power-law index to the default values used in compiling the 3XMM catalogue,

<http://www.sr.bham.ac.uk/xmm2/>.

⁸The *NH Tool* is available at <http://www.nsatlas.org>.

⁹We remind that in such cases (as investigated by Watson et al. 2009) varying the shape of the power-law would result in a flux change up to a few percent.

i.e. $n_H = 3 \times 10^{20} \text{ cm}^{-2}$ and $\Gamma = 1.7$.

When we noted the typical signatures of obscured sources (usually active galactic nuclei of the Seyfert 2 type with $n_H > 10^{22}$, see e.g. Matt. 2002 for a review), we used a simplified version of the models described in LaMassa et al. (2014), i.e. `const*phabs*pcfabs*powerlaw` (within XSPEC), where `pcfabs` represents a partial covering fraction absorption depending on the photo-electric cross-section, n_H^{int} the intrinsic hydrogen column density and f a covering factor ranging between 0 (free source) to 1 (a full spherical envelope surrounding the source). We verified that this simple model results in acceptable fits and in best fit parameters consistent with those found by using more sophisticated models.

The results of this analysis are reported in Table 2. Here, for any source of the GiX catalogue we give the absorbed (third column) and unabsorbed (fourth column) flux in the 0.2 – 12 keV energy band (i.e., the *XMM-Newton* entire range) obtained by fitting the associated spectra within the XSPEC package with one of the models (second column) described above. When the flux estimate lacks of the (90% confidence level) errors, the corresponding number represents an upper-limit. We also give the hydrogen column density n_H (fifth column), the power-law index Γ (sixth column), as well as the n_H^{int} and f values for the B model sources (last two columns).

In the latter case the n_H^{int} estimates confirmed the idea of obscured AGN as the sources of the spectra.

4. Candidate massive black holes from the X-ray/Radio fundamental plane

We searched for radio counterparts by cross-matching our sample of X-ray nuclear sources (consistent with the galaxy center, within the positional errors) with the FIRST and NVSS catalogues at 1.4 GHz, as well as RG2007 at 1.4 GHz, 4.9 GHz and 8.4 GHz. Consequently, we found 19 X-ray sources (characterized by an X-ray detection likelihood larger than $\simeq 16.6$) correlating in position¹⁰

¹⁰ The distance between an X-ray source and its radio counterpart was evaluated by using the well known haversine formula while the associated error was calculated by propagating correctly the uncertainties on both the celestial coordinates. In this respect, the error on the position of a radio source in the FIRST catalogue was derived by using the empirical relation described in <http://sundog.stsci.edu/first/catalogs/readme.13jun05.html#evlcalibration> and, then, associated to the right ascension and declination, respectively. For the NVSS

with radio ones within $\simeq 2''$, apart from sources #28 and #33 which have radio counterparts at distance of $\simeq 4.2''$ (NVSS J125837 + 271033) and $\simeq 4.5''$ (NVSS J120222 + 295143), respectively. Since the positional errors (see Table 3) on the separation between these two X-ray sources and their radio counterparts are $\simeq 4''$ and $\simeq 2''$, the association is less robust. Anyway, we maintain sources #28 and #33 in our final list of massive candidate black holes.

In Figure 1, we give, for each source, the Sloan r band image (color inverted and in log scale) centered on the galaxy target. In each panel, the source position is indicated by a red circle having radius of $3''$ centered on the X-ray source coordinates.

In the case of FIRST and NVSS, from the 1.4 GHz radio flux density of the identified sources, we can estimate the 5 GHz flux assuming a flat spectrum¹¹, i.e. $F(\nu) \propto \nu^{-\alpha_R}$ with $\alpha_R = 0$, while for source #1 (Mrk 1303 also known as UM 444) the radio flux was directly taken from Table 2 in RG2007.

Then, after restricting the X-ray flux of our sources to the 2 – 10 keV band, we used the Merloni et al. (2003) fundamental plane, i.e.

$$\log(M_{BH}) \simeq 16.3 + \log(D) + 1.28(\log(F_{5\text{ GHz}}) - 0.60 \log(F_{2-10\text{ keV}})) \pm 1.06 \quad (1)$$

in order to get an estimate of the mass of the candidate black holes. In the previous relation, D is the source distance expressed in Mpc and the last term corresponds to the intrinsic scatter in the fundamental plane relation. In Table 3, we give the main data corresponding to the 19 sources of interest, i.e. the ID used in the present paper, the galaxy distance (in Mpc) as derived from the NASA Sloan Atlas, the J2000 coordinates (in degrees) of the X-ray target and the positional error (Err^X), the X-ray flux in the 2 – 10 keV band, the coordinates of the radio counterpart along with the positional uncertainty (Err^{radio}), the 5 GHz flux, the X-ray and radio source separation and associated error, the mass of the black hole, the mass of the galaxy M_{gal} as derived using the SDSS data via the *kcorrect* code of Blanton & Roweis (2007), and the dynamical mass

sources, the error in position was simply read from the catalogue itself. In the case of RG2007, the positional error was obtained by summing in quadrature the respective uncertainties in the celestial coordinates.

¹¹ We note that the obtained black hole mass values slightly depend on the index α_R characterizing the radio spectral energy distribution. In particular, the black hole mass scales with the factor $(1.4\text{GHz}/5\text{GHz})^{1.28\alpha_R}$, get reducing by $\simeq 50\%$ for $\alpha_R = 0.4$.

M_{gal}^{dyn} obtained by using the mass estimator described in Padmanabhan et al. (2004). In particular, the three-dimensional velocity v of a test object orbiting a mass $M(r)$ at distance r is simply given by

$$v^2(r) = \frac{GM(r)}{r}. \quad (2)$$

To compute the dynamical mass, one must choose a characteristic radius and relate the observed dispersion velocity σ at that radius to the above circular velocity. Here, we fixed r to the Petrosian 50% light radius (R_{50} as derived from SDSS r band) and assumed $v^2(r) = \eta\sigma^2$, where η is 2 or 3 in case of spirals or ellipticals, respectively.

Following Bernardi et al. (2003) (and references therein) we applied an empirical correction to the measured dispersion σ to account for the fact that the dispersion velocity estimated by the SDSS spectra is not at the Petrosian 50% radius but at the fiber diameter of $3''$. Then the corrected dispersion velocity is

$$\sigma_{corr} = \sigma \left(\frac{8r_{fiber}}{r_{eff}} \right)^{0.04}, \quad (3)$$

where $r_{fiber} \simeq 1.5''$ and r_{eff} is the effective radius of the galaxy measured in arcseconds which we set again equal to R_{50} . Finally, our dynamical mass estimator reads out as

$$M_{gal}^{dyn} = \frac{\eta\sigma_{corr}^2 R_{50}}{G}. \quad (4)$$

The above algorithm (except for #40 and #51) allows one to estimate the dynamical mass of the galaxy, but this value has not to be considered too robust as other mass estimators could give different values. In Table 3, we always assumed $\eta = 3$. In the last column of Table 3 we also give the X-ray accretion efficiency ϵ_X which represents a lower limit to the true accretion efficiency value, i.e.

$$\epsilon_X \simeq \frac{L_{0.2-12\text{ keV}}}{L_{Edd}}, \quad (5)$$

where $L_{Edd} \simeq 1.38 \times 10^{38} \left(\frac{M_{BH}}{M_\odot} \right) \text{ erg s}^{-1}$.

In all the cases for which the X-ray target is found within a distance of $\simeq 3''$ from the optical centre, the corresponding source was considered to be a nuclear black hole candidate. When the distance is greater than $3''$, the source could not be a non-nuclear black hole candidate (possibly a ULX, see in this respect Swartz et al. 2008 for a discussion on the number of ULXs found in low mass galaxies). Note also that for

sources #35 (NGC 4117) and #50 (NGC 4395), our estimate of the candidate black hole mass is a factor ≈ 10 larger (but still consistent due to the large intrinsic scatter of the fundamental plane relation) than the values derived by Woo & Urry (2002) and den Brok et al. (2015), respectively, when studying the gas dynamics in the galaxies and/or using the virial assumption for the broad emission lines while determining the broad-line region size from either reverberation mapping or optical luminosity.

In Figure 2, we give the X -ray/radio fundamental plane (adapted from Merloni et al. 2003) superimposing our results (dodger blue empty stars). Here, we consider Galactic BHs (GBH), Liners-Transition and quasi stellar objects (L-T and QSO, respectively), Seyfert nuclei (Sy) and undefined sources. As evident, our sample lies on the X -ray/radio fundamental plane so that we are justified in using eq. (1) to infer the black hole mass. This is also in accordance to Gültekin et al. 2014 who, by studying a sample of low-mass AGNs in the X -ray and radio bands, concluded that the fundamental plane is a good mass estimator and is suitable for searching for IMBH candidates. In this respect, we also consider in the same figure the IMBH candidates (filled black circles, and mass less than $10^{6.3} M_{\odot}$) corresponding to the eleven low-mass AGNs in Gültekin et al. 2014. We also insert the observations corresponding to IMBHs (open circles) supposed to be hosted in selected globular clusters and nearby dwarf galaxies (Nucita et al. 2008; Wrobel et al. 2011; Webb et al. 2012; Nyland et al. 2012; Nucita et al. 2013a,b; Manni et al. 2015; Mezcua et al. 2015; Earnshaw 2016; Earnshaw et al. 2016), whose associated mass can be determined via dynamical methods.

Table 1.: The GiX catalogue obtained by cross-correlating the NASA-Sloan Atlas and the 3XMM-DR5 databases. Columns are: our identifier, the *XMM*-Newton observation ID, the NASA-Sloan Atlas ID, the common target name, the (J2000) optical coordinates associated to the galaxies, the distance (in arcseconds) between the Sloan source and its *X*-ray counterpart, the galaxy mass, the quality flag associated to the *X*-ray source, and its counts as derived by the 3XMM-DR5 catalogue. Source # 42 was also in the *XMM*-Newton field of view during the observation 0550960601. However, since this particular observation was affected by large flares for most of the exposure window, we avoided to use it.

Src #	OBSID	NSAID	Name	RA (J2000)	DEC (J2000)	s	$\frac{M_{gal}}{M_{\odot}}$	SF	Counts
1	0303561801	1120	Mrk 1303	175.05513	-0.41171	0.6	$7.99 \times 10^{+08}$	0	42.8 ± 8.7
2	0124710501	103903	Mrk 58	194.77209	27.64444	2.7	$8.08 \times 10^{+09}$	0	117.2 ± 20.0
3	0108860501	84201	2MASX J08193880+2103521	124.91171	21.06439	2.1	$2.11 \times 10^{+09}$	0	42.3 ± 10.0
4	0041180801	163589	2MASX J13293557+1141515	202.39807	11.69777	1.9	$9.48 \times 10^{+09}$	0	62.4 ± 14.2
5	0205910101	88939	NVSS J130916+292202	197.31704	29.36766	2.0	$7.31 \times 10^{+09}$	0	233.4 ± 21.0
6	0403150201	103917	2MASX J12581865+2718387	194.57766	27.31082	1.0	$4.53 \times 10^{+09}$	0	158.7 ± 20.8
7	0551280101	113915	ACO 1413	178.99342	23.45862	0.6	$4.66 \times 10^{+09}$	0	120.7 ± 19.8
8	0150010601	60414	2MASX J12093747+4219081	182.40619	42.31888	1.8	$9.44 \times 10^{+09}$	0	29.6 ± 8.8
9	0200530401	40521	ANT Galaxy	164.21248	6.90612	2.4	$6.06 \times 10^{+09}$	0	128.0 ± 15.1
10	0402370101	50679	2XMMi J092720.4+362407	141.83526	36.40184	1.1	$5.01 \times 10^{+08}$	0	160.3 ± 17.9
11	0404120101	169920	IC 800	188.48607	15.35484	0.8	$7.47 \times 10^{+09}$	0	231.6 ± 23.0
12	0679381101	37345	SDSS J112910.56+582309.0	172.29392	58.38587	2.5	$3.10 \times 10^{+09}$	0	35.5 ± 8.4
13	0101640901	97727	SDSS J153510.78+232409.4	233.79493	23.40266	1.6	$1.82 \times 10^{+09}$	0	41.2 ± 9.3
14	0204400101	162072	2XMM J123519.9+393110	188.83349	39.51918	2.3	$1.51 \times 10^{+08}$	0	207.4 ± 18.1
15	0652310701	103933	Mrk 55	194.35521	27.40457	0.2	$6.07 \times 10^{+09}$	0	60.7 ± 12.0
16	0204650301	88791	SDSS J113939.20+315320.3	174.91338	31.88897	1.9	$7.21 \times 10^{+09}$	0	26.1 ± 7.0
17	0124710401	104152	7W 1258+27W06	195.14032	27.63774	2.6	$5.44 \times 10^{+09}$	0	58.2 ± 13.6
18	0504101701	58897	2MASX J10181928+3722419	154.58017	37.37842	0.2	$7.63 \times 10^{+09}$	0	225.8 ± 17.7
19	0400570101	15235	2XMMi J144012.6+024744	220.05294	2.79542	0.7	$2.87 \times 10^{+09}$	0	377.7 ± 23.4
20	0150010601	60412	SDSS J120900.89+422830.9	182.25372	42.47526	2.1	$3.42 \times 10^{+09}$	0	77.9 ± 12.2
21	0112270601	118256	2MASX J12035600+2025499	180.98330	20.43044	1.1	$1.05 \times 10^{+10}$	0	27.7 ± 7.2
22	0505210601	99202	Mrk 695	240.71243	15.96107	2.0	$4.00 \times 10^{+09}$	0	95.8 ± 16.6
23	0094383201	162694	Mrk 447	194.54165	24.34891	3.0	$4.20 \times 10^{+09}$	0	18.4 ± 5.7
24	0109462201	42891	2MASX J13070847+5357446	196.78517	53.96242	1.0	$1.76 \times 10^{+09}$	0	37.8 ± 8.1
25	0103260801	157523	FIRST J095310.3+075224	148.29327	7.87361	1.0	$8.39 \times 10^{+09}$	0	256.1 ± 19.3
26	0606030101	37086	MCG+10-16-025	163.86892	57.90620	2.0	$7.47 \times 10^{+09}$	0	105.0 ± 16.7
27	0025540301	84441	SDSS J083749.83+254804.8	129.45764	25.80136	0.8	$5.83 \times 10^{+09}$	0	73.4 ± 11.1
28	0403150201	103591	NVSS J125837+271033	194.65534	27.17655	1.8	$5.25 \times 10^{+09}$	0	81.2 ± 16.8
29	0504101501	19510	2MASX J13463217+6423247	206.63399	64.39041	0.6	$8.89 \times 10^{+09}$	0	168.9 ± 17.3
30	0202730101	108428	SDSS J102217.95+212642.8	155.57480	21.44524	1.2	$5.94 \times 10^{+09}$	0	704.8 ± 30.9
31	0674810701	158462	NGC 3259	158.14524	65.04115	0.8	$8.92 \times 10^{+09}$	0	274.8 ± 21.3
32	0674810601	63442	2MASS J16315959+2437403	247.99833	24.62786	0.2	$6.79 \times 10^{+09}$	0	1105.3 ± 36.9
33	0555060301	102563	NVSS J120222+295143	180.59389	29.86176	2.9	$1.01 \times 10^{+10}$	0	33.4 ± 8.3
34	0124710801	104185	2XMM J130200.1+274657	195.50061	27.78271	0.8	$9.35 \times 10^{+09}$	0	3808.8 ± 65.8
35	0655800501	60658	NGC 4117	181.94215	43.12635	0.2	$3.91 \times 10^{+09}$	0	326.3 ± 21.8
36	0204651201	41675	NGC 3982	179.11726	55.12528	1.8	$1.00 \times 10^{+10}$	0	1787.0 ± 50.4
37	0502211401	103006	2MASX J12221536+2821231	185.56407	28.35661	0.3	$5.44 \times 10^{+09}$	0	88.4 ± 11.9
38	0504102001	156668	2MASX J08244333+2959238	126.18034	29.98987	0.1	$9.41 \times 10^{+09}$	0	4081.4 ± 68.7
39	0504100201	74152	2MASX J09591475+1259161	149.81153	12.98789	0.4	$4.68 \times 10^{+09}$	0	7322.1 ± 90.6
40	0651100401	45387	Mrk 477	220.15872	53.50453	0.3	$1.00 \times 10^{+10}$	0	3204.3 ± 60.4
41	0400570201	27397	UGC 6192	167.30166	61.39641	1.4	$8.21 \times 10^{+08}$	1	61.9 ± 11.9
42	0067340601	73400	—	241.71258	8.15796	0.9	$1.50 \times 10^{+08}$	1	164.5 ± 24.6
43	0404410101	62285	—	18.85011	0.63552	2.0	$1.82 \times 10^{+08}$	1	124.5 ± 23.8
44	0210280101	84591	2XMM J085735.4+274607	134.39726	27.76813	2.6	$2.88 \times 10^{+08}$	1	512.3 ± 29.6
45	0147210301	99052	2XMM J160531.8+174825	241.38272	17.80726	0.5	$1.74 \times 10^{+09}$	1	136.2 ± 15.5
46	0111260201	165958	NGC 5879	227.44484	57.00024	1.5	$8.14 \times 10^{+09}$	1	352.4 ± 23.3
47	0303550901	10045	2XMMi J082912.8+500652	127.30277	50.11465	0.4	$4.12 \times 10^{+09}$	1	24289.5 ± 172.5
48	0674811101	52675	2MASX J12234282+5814459	185.92846	58.24623	0.2	$2.92 \times 10^{+09}$	1	7622.3 ± 92.8
49	0149010201	47963	IC 2461	139.99178	37.19125	0.8	$8.13 \times 10^{+09}$	1	19663.3 ± 149.9
50	0112521901	89394	NGC 4395	186.45362	33.54687	0.1	$1.27 \times 10^{+09}$	1	12175.3 ± 116.2
51	0051760101	14301	2XMM J124635.3+022209	191.64688	2.36911	0.1	$6.86 \times 10^{+09}$	1	82587.9 ± 296.8

Table 2:: The absorbed (third column) and unabsorbed (fourth column) flux in the 0.2 – 12 keV energy band for each of the GiX catalogue entries. The X-ray spectra were fitted within the XSPEC package using the model indicated in the second column (see text for details) and the values of the hydrogen column density, power-law index, intrinsic hydrogen column density and covering fraction factor shown in the last four columns, respectively. For source # 51 (labeled with an asterisk), considering a single power-law resulted in residuals at low energies. The residuals disappeared when considering a black-body component with temperature of $kT \approx 0.14$ keV.

Src #	Model	$F_{0.2-12keV}^{Abs}$ erg s ⁻¹ cm ⁻²	$F_{0.2-12keV}^{UnAbs}$ erg s ⁻¹ cm ⁻²	n_H 10 ²⁰ cm ⁻²	Γ	n_H^{int} 10 ²² cm ⁻²	f
1	A	$2.15^{+1.2}_{-2.5} \times 10^{-14}$	2.3×10^{-14}	2.4	1.7		
2	A	$1.7^{+2.5}_{-0.8} \times 10^{-14}$	1.9×10^{-14}	0.9	$2.28^{+0.96}_{-0.48}$		
3	A	$2.8^{+1.8}_{-1.7} \times 10^{-14}$	3.2×10^{-14}	4.3	1.7		
4	A	$1.2^{+0.7}_{-0.7} \times 10^{-14}$	1.3×10^{-14}	3.0	1.7		
5	A	$1.2^{+0.4}_{-0.5} \times 10^{-14}$	1.2×10^{-14}	1.0	1.7		
6	A	$1.4^{+0.5}_{-0.5} \times 10^{-14}$	1.6×10^{-14}	3.0	1.7		
7	A	$1.1^{+0.7}_{-0.7} \times 10^{-14}$	1.2×10^{-14}	2.1	1.7		
8	A	$2.0^{+2.1}_{-1.9} \times 10^{-14}$	2.2×10^{-14}	1.7	1.7		
9	A	$2.4^{+1.7}_{-0.6} \times 10^{-14}$	3.3×10^{-14}	3.0	$2.41^{+0.82}_{-0.61}$		
10	A	$2.9^{+1.5}_{-1.0} \times 10^{-14}$	2.9×10^{-14}	1.4	$1.18^{+0.40}_{-0.38}$		
11	A	$1.7^{+0.3}_{-0.3} \times 10^{-14}$	1.8×10^{-14}	3.0	1.7		
12	A	$2.7^{+1.5}_{-1.6} \times 10^{-14}$	2.8×10^{-14}	1.0	1.7		
13	A	$1.1^{+0.6}_{-0.5} \times 10^{-14}$	1.2×10^{-14}	4.3	1.7		
14	A	$2.9^{+1.2}_{-0.6} \times 10^{-14}$	3.1×10^{-14}	1.5	$1.79^{+0.45}_{-0.36}$		
15	A	$6.2^{+2.6}_{-2.8} \times 10^{-14}$	6.5×10^{-14}	0.9	1.7		
16	A	$3.2^{+7.6}_{-1.9} \times 10^{-14}$	3.7×10^{-14}	2.0	$1.82^{+1.54}_{-0.87}$		
17	A	4.3×10^{-14}	4.4×10^{-14}	0.9	1.7		
18	A	$4.2^{+0.7}_{-0.7} \times 10^{-14}$	5.3×10^{-14}	1.3	$2.83^{+0.27}_{-0.24}$		
19	A	$2.8^{+0.5}_{-0.5} \times 10^{-14}$	3.1×10^{-14}	2.9	1.7		
20	A	$3.2^{+1.2}_{-1.2} \times 10^{-14}$	3.5×10^{-14}	3.0	1.7		
21	A	$3.3^{+2.8}_{-2.8} \times 10^{-14}$	3.6×10^{-14}	3.0	1.7		
22	A	$4.5^{+1.9}_{-2.8} \times 10^{-14}$	5.0×10^{-14}	3.4	1.7		
23	A	$3.5^{+2.4}_{-2.4} \times 10^{-14}$	3.8×10^{-14}	3.0	1.7		
24	A	$3.6^{+1.8}_{-1.8} \times 10^{-14}$	4.0×10^{-14}	3.0	1.7		
25	A	$2.8^{+0.7}_{-0.7} \times 10^{-14}$	3.8×10^{-14}	3.0	$2.38^{+0.63}_{-0.47}$		
26	A	$5.0^{+3.4}_{-1.7} \times 10^{-14}$	5.1×10^{-14}	0.6	$1.44^{+0.47}_{-0.40}$		
27	A	$6.3^{+5.8}_{-2.5} \times 10^{-14}$	6.6×10^{-14}	3.6	$1.29^{+0.56}_{-0.55}$		
28	A	$5.4^{+3.1}_{-3.1} \times 10^{-14}$	6.0×10^{-14}	3.0	1.7		
29	A	$2.3^{+1.7}_{-0.8} \times 10^{-14}$	2.5×10^{-14}	2.2	$1.48^{+0.78}_{-0.83}$		
30	A	$8.1^{+1.2}_{-1.0} \times 10^{-14}$	8.6×10^{-14}	2.0	$1.59^{+0.12}_{-0.12}$		
31	B	1.4×10^{-13}	1.5×10^{-13}	1.7	$2.19^{+0.18}_{-0.23}$	$18.36^{+7.37}_{-5.71}$	$0.98^{+0.01}_{-0.1}$
32	B	$1.4^{+0.2}_{-0.7} \times 10^{-13}$	1.9×10^{-13}	3.8	$2.35^{+0.13}_{-0.13}$	$18.52^{+7.15}_{-12.31}$	$0.70^{+0.23}_{-0.30}$
33	A	9.2×10^{-14}	9.7×10^{-14}	1.6	1.7		
34	A	$4.3^{+0.1}_{-0.1} \times 10^{-13}$	6.0×10^{-13}	0.9	1.7		
35	B	$4.3^{+1.1}_{-1.8} \times 10^{-13}$	4.6×10^{-13}	1.4	1.7	$51.58^{+13.91}_{-12.21}$	$0.98^{+0.01}_{-0.02}$
36	B	$3.5^{+2.5}_{-3.0} \times 10^{-13}$	4.2×10^{-13}	1.2	$3.08^{+0.31}_{-0.35}$	$21.23^{+12.11}_{-6.77}$	$0.985^{+0.012}_{-0.050}$
37	A	$1.8^{+0.6}_{-0.7} \times 10^{-13}$	1.9×10^{-13}	1.8	1.7		
38	B	$1.4^{+0.1}_{-0.2} \times 10^{-12}$	1.5×10^{-12}	3.8	$1.30^{+0.06}_{-0.15}$	$17.71^{+1.56}_{-1.67}$	$0.992^{+0.006}_{-0.042}$
39	B	$1.3^{+0.1}_{-0.1} \times 10^{-12}$	1.3×10^{-12}	3.2	$1.90^{+0.05}_{-0.12}$	$0.92^{+0.08}_{-0.09}$	> 0.945
40	B	$2.3^{+0.2}_{-0.2} \times 10^{-12}$	2.3×10^{-12}	1.3	$1.75^{+0.05}_{-0.10}$	$25.84^{+3.03}_{-2.20}$	$0.990^{+0.008}_{-0.040}$
41	A	$4.2^{+3.6}_{-3.8} \times 10^{-15}$	4.4×10^{-15}	0.7	1.7		
42	A	$4.9^{+0.5}_{-2.9} \times 10^{-14}$	5.0×10^{-14}	4.0	$1.04^{+0.73}_{-0.63}$		
43	A	$5.5^{+5.7}_{-2.8} \times 10^{-14}$	5.8×10^{-14}	3.2	$1.37^{+1.17}_{-0.85}$		
44	A	$2.6^{+0.8}_{-0.5} \times 10^{-14}$	2.8×10^{-14}	3.1	$1.70^{+0.17}_{-0.17}$		
45	A	$3.5^{+13.9}_{-2.2} \times 10^{-14}$	3.8×10^{-14}	3.5	$1.54^{+1.46}_{-1.05}$		
46	A	$4.8^{+1.1}_{-0.7} \times 10^{-14}$	5.5×10^{-14}	1.5	$2.20^{+0.32}_{-0.35}$		
47	A	$2.06^{+0.03}_{-0.04} \times 10^{-12}$	3.2×10^{-12}	4.0	$2.61^{+0.25}_{-0.02}$		
48	A	$2.9^{+0.1}_{-0.1} \times 10^{-12}$	3.1×10^{-12}	1.2	$1.83^{+0.05}_{-0.03}$		
49	B	$5.4^{+0.1}_{-0.2} \times 10^{-12}$	5.4×10^{-12}	1.6	$0.60^{+0.03}_{-0.05}$	$4.30^{+0.22}_{-0.05}$	$0.995^{+0.005}_{-0.005}$

Continued on Next Page...

Table 2 – Continued

Src #	Model	$F_{0.2-12keV}^{Abs}$ $\text{erg s}^{-1} \text{cm}^{-2}$	$F_{0.2-12keV}^{UnAbs}$ $\text{erg s}^{-1} \text{cm}^{-2}$	n_H 10^{20}cm^{-2}	Γ	n_H^{int} 10^{22}cm^{-2}	f
50	B	$8.4^{+0.2}_{-0.3} \times 10^{-12}$	8.4×10^{-12}	1.3	$0.91^{+0.03}_{-0.05}$	$4.81^{+0.32}_{-0.29}$	$0.975^{+0.015}_{-0.025}$
51*	A	$1.28^{+0.02}_{-0.03} \times 10^{-11}$	1.8×10^{-11}	1.8	$2.91^{+0.03}_{-0.03}$		

Table 3:: A sub-sample of the GiX sources correlating in position with the 1.4 GHz sources of the FIRST, NVSS and RG2007 catalogues. For these sources we give the galaxy distance, the X -ray position and associated error, the unabsorbed flux in 2 – 10 keV band, the radio counterpart position and error, the 5 GHz flux, the separation (and associated uncertainty) between the X -ray and the radio source, the estimated central black hole mass, the mass of the galaxy as derived by the SDSS observations, the dynamical mass and the black hole X -ray accretion efficiency ϵ_X (see text for details). Note that the error associated to the black hole mass is 1.06 dex as derived from the fundamental plane relation.

Src #	D Mpc	RA ^X (J2000) °	DEC ^X (J2000) °	Err ^X "	F _{2–10keV} erg s ⁻¹ cm ⁻²	RA ^{radio} (J2000) °	DEC ^{radio} (J2000) °	Err ^{radio} "	F _{5GHz} erg s ⁻¹ cm ⁻²	s "	log M _{BH} M _⊙	log M _{gal} M _⊙	log M _{gal} ^{dyn} M _⊙	ε _X
1	90.4	175.05527	-0.41180	1.7	1.2 × 10 ⁻¹⁴	175.05500	-0.41167	1.8	7.1 × 10 ⁻¹⁷	1.1 ± 2.3	8.28	8.90	9.11	8.6 × 10 ⁻⁷
2	74.4	194.77145	27.64394	1.6	5.1 × 10 ⁻¹⁵	194.77195	27.64426	1.2	2.1 × 10 ⁻¹⁷	2.0 ± 1.7	7.80	9.91	8.72	1.4 × 10 ⁻⁶
5	86.0	197.31680	29.36716	0.9	6.3 × 10 ⁻¹⁵	197.31708	29.36746	1.0	2.3 × 10 ⁻¹⁷	1.4 ± 1.0	7.84	9.86	9.21	1.1 × 10 ⁻⁶
6	101.5	194.57782	27.31107	1.2	8.0 × 10 ⁻¹⁵	194.57749	27.31093	0.6	2.5 × 10 ⁻¹⁷	1.2 ± 1.2	7.87	9.66	9.65	1.9 × 10 ⁻⁶
15	66.4	194.35523	27.40452	1.5	3.3 × 10 ⁻¹⁴	194.35525	27.40492	1.1	1.5 × 10 ⁻¹⁷	1.4 ± 1.5	6.95	9.78	9.93	2.8 × 10 ⁻⁵
22	144.5	240.71251	15.96162	1.7	2.6 × 10 ⁻¹⁴	240.71273	15.96104	1.1	1.8 × 10 ⁻¹⁷	2.2 ± 1.7	7.46	9.60	9.42	3.1 × 10 ⁻⁵
24	120.7	196.78472	53.96239	1.8	2.1 × 10 ⁻¹⁴	196.78549	53.96223	0.9	2.1 × 10 ⁻¹⁷	1.7 ± 1.2	7.52	9.24	9.50	1.5 × 10 ⁻⁵
25	167.1	148.29339	7.87334	0.7	9.1 × 10 ⁻¹⁵	148.29320	7.87349	0.8	3.7 × 10 ⁻¹⁷	0.9 ± 0.9	8.28	9.92	10.32	4.8 × 10 ⁻⁶
28	105.0	194.65522	27.17606	1.9	3.1 × 10 ⁻¹⁴	194.65653	27.17589	3.9	7.8 × 10 ⁻¹⁷	4.2 ± 3.8	8.08	9.72	9.52	4.8 × 10 ⁻⁶
31	23.0	158.14528	65.04093	0.7	1.1 × 10 ⁻¹³	158.14563	65.04108	9.4	1.1 × 10 ⁻¹⁶	0.8 ± 2.8	7.19	9.95	9.79	4.5 × 10 ⁻⁶
33	42.8	180.59480	29.86180	2.0	5.1 × 10 ⁻¹³	180.59342	29.86145	0.4	1.0 × 10 ⁻¹⁶	4.5 ± 1.8	6.89	10.00	9.83	1.9 × 10 ⁻⁵
35	13.0	181.94222	43.12635	0.7	2.8 × 10 ⁻¹³	181.94208	43.12643	1.4	2.7 × 10 ⁻¹⁷	0.5 ± 1.0	5.84	9.59	9.39	9.7 × 10 ⁻⁵
36	15.3	179.11786	55.12564	0.7	1.1 × 10 ⁻¹³	179.11730	55.12529	0.7	4.3 × 10 ⁻¹⁷	1.7 ± 0.6	6.47	10.00	9.72	2.8 × 10 ⁻⁵
38	104.4	126.18034	29.98986	0.2	1.1 × 10 ⁻¹²	126.18044	29.98994	0.5	3.3 × 10 ⁻¹⁷	0.4 ± 0.4	6.42	9.97	10.01	5.4 × 10 ⁻³
39	141.0	149.81165	12.98786	0.3	9.5 × 10 ⁻¹³	149.81155	12.98791	0.7	2.8 × 10 ⁻¹⁶	0.4 ± 0.7	7.78	9.67	9.99	3.7 × 10 ⁻⁴
40	151.5	220.15871	53.50445	0.3	1.6 × 10 ⁻¹²	220.15876	53.50438	1.7	8.1 × 10 ⁻¹⁶	0.3 ± 0.6	8.22	10.00	--	2.7 × 10 ⁻⁴
49	30.9	139.99161	37.19108	0.3	3.9 × 10 ⁻¹²	139.99157	37.19101	0.3	4.0 × 10 ⁻¹⁷	0.3 ± 0.3	5.56	9.91	10.01	1.2 × 10 ⁻²
50	4.4	186.45360	33.54686	0.2	6.3 × 10 ⁻¹²	186.45383	33.54680	0.5	1.7 × 10 ⁻¹⁷	0.7 ± 0.4	4.07	9.10	12.16	1.1 × 10 ⁻²
51	197.7	191.64686	2.36912	0.2	1.9 × 10 ⁻¹²	191.64712	2.36929	2.2	2.7 × 10 ⁻¹⁷	1.1 ± 1.9	6.39	9.84	--	2.4 × 10 ⁻¹

5. Conclusions

In this paper we presented *GiX*, a sample of X -ray detected low mass galaxies with mass $\lesssim 10^{10} M_{\odot}$. The catalogue has been obtained by cross-correlating the NASA-Sloan Atlas with the 3XMM catalogue and consists of 51 X -ray emitting low mass galaxies. We also matched the catalogue with the FIRST, NVSS and RG2007 databases and found 19 sources with a radio counterpart. Although dedicated follow up observations would be required in order to disentangle the nature of the sources, the targets, which are well consistent in position with the galactic center regions, are characterized by an X -ray and radio luminosities that distribute according to the fundamental plane relation of Merloni et al. (2003). This fact allows one to use the previous relation (which has primarily a statistical nature) as a tool to estimate the mass of the central black hole candidates. Of course, the error associated to the estimated mass cannot be smaller than that (± 1.06) derived by Merloni et al. (2003) (to which we refer for more details) using the intrinsic scatter (i.e. the dispersion of the interesting variables) of the fundamental plane itself.

When performing this calculation, we found black hole candidates with mass in the range $\approx 10^4 - 2 \times 10^8 M_{\odot}$ (see the seventh column in Table 3), with eight candidates having mass below $10^7 M_{\odot}$.

By comparing the observed 0.2–12 keV luminosity with the Eddington limit, we found that all the sources appear to radiate with efficiency in the range $\approx 0.2 - 10^{-6}$, with only 3 sources over 19 emitting with very high efficiency ($\epsilon_X \gtrsim 10^{-2}$) and 3 black hole candidates having intermediate values of efficiency in the range $10^{-2} - 10^{-4}$.

A similar analysis has been recently performed by Lemons et al. (2015) by cross-correlating a sample of dwarfs with the Chandra Source Catalogue and finding 19 galaxies with a number of point-like X -ray sources with hard spectra and 2–10 keV luminosities between $10^{37} \text{ erg s}^{-1}$ and $10^{40} \text{ erg s}^{-1}$, i.e. in the typical range of power emitted by stellar-mass X -ray binaries and massive black holes accreting at relatively low Eddington rate.

By using the data reported in Table 3, and having in mind the large uncertainties due to the intrinsic scatter of the fundamental plane, it is interesting to note that 7 targets have M_{gal}/M_{BH} in the range $[1, 100]$, 5 targets have M_{gal}/M_{BH} in the range $]100, 1000]$, while 7 entries have M_{gal}/M_{BH} larger than or equal to 1000.

In the first case, the galaxies seem to be outliers in the black hole-host galaxy scaling relations. This is particularly true for source #1 (NGC 1303) for which the galaxy to black hole mass ratio is of the order of ≈ 4 . As a matter of fact, recently Seth et al. (2014) (but see also Reines 2014) analyzed the adaptive optics kinematic data of M60-UCD1 (an ultra-compact dwarf galaxy with mass $\approx (1.2 \pm 0.4) \times 10^8 M_{\odot}$). In order to explain the observed stellar velocities and the light distribution within the galaxy, these authors must assume the presence of a central massive black hole with mass of $2.1^{+1.2}_{-0.7} \times 10^7 M_{\odot}$, thus resulting in a galaxy to black hole mass ratio M_{gal}/M_{BH} between ≈ 2.3 and ≈ 11 (with a central value of ≈ 5.7)¹². Although the discovery of such massive object is impressive, recent works (see, e.g., Reines et al. 2013) already suggested the existence of massive black holes in dwarf galaxies when using virial techniques. Note however that these authors, using a sample of 151 dwarf galaxies that exhibit optical spectroscopic signatures of accreting black holes, found black holes candidates with masses in the range $10^5 - 10^6 M_{\odot}$ and median $2 \times 10^5 M_{\odot}$, i.e. significantly smaller than those derived in this work using correlation between X -ray and radio data only. As a matter of fact, our sample is characterized by black hole candidates with mass in the range $10^{4.1} - 10^{8.3} M_{\odot}$ and median value $\approx 3 \times 10^7 M_{\odot}$. However, we remind that these values were estimated assuming a radio spectral index $\alpha_R = 0$ from which the black hole mass slightly depends on (see Sect. 4).

Of course, X -ray emitting sources in low-mass galaxies may have had a key role in the evolution of such systems, thus making urgent a theoretical background able to explain how such massive objects formed. In this respect, next coming optical and X -ray surveys, as those planned to be performed by Euclid and eRosita, will certainly help in solving this puzzling problem. Euclid, whose primary goal is to map the geometry of the dark universe and to constrain the dark energy content (see, e.g. Refreiger et al. 2010 and Cimatti & Scaramella 2012) by performing a ≈ 20000 square degrees survey down to ≈ 24.5 AB magnitude, will allow also to detect (as a by-product) $\approx 10^5$ dwarf galaxies up to ≈ 100 Mpc Laureijs et al. (2011). During the life-time of the Euclid mission, the eRosita (extended ROentgen Survey with an Imaging Tele-

¹²Seth et al. (2014) explained their finding postulating that M60-UCD1 is the stripped nucleus of a galaxy due to the interaction with the galaxy M60 which probably happened about 10 billions years ago.

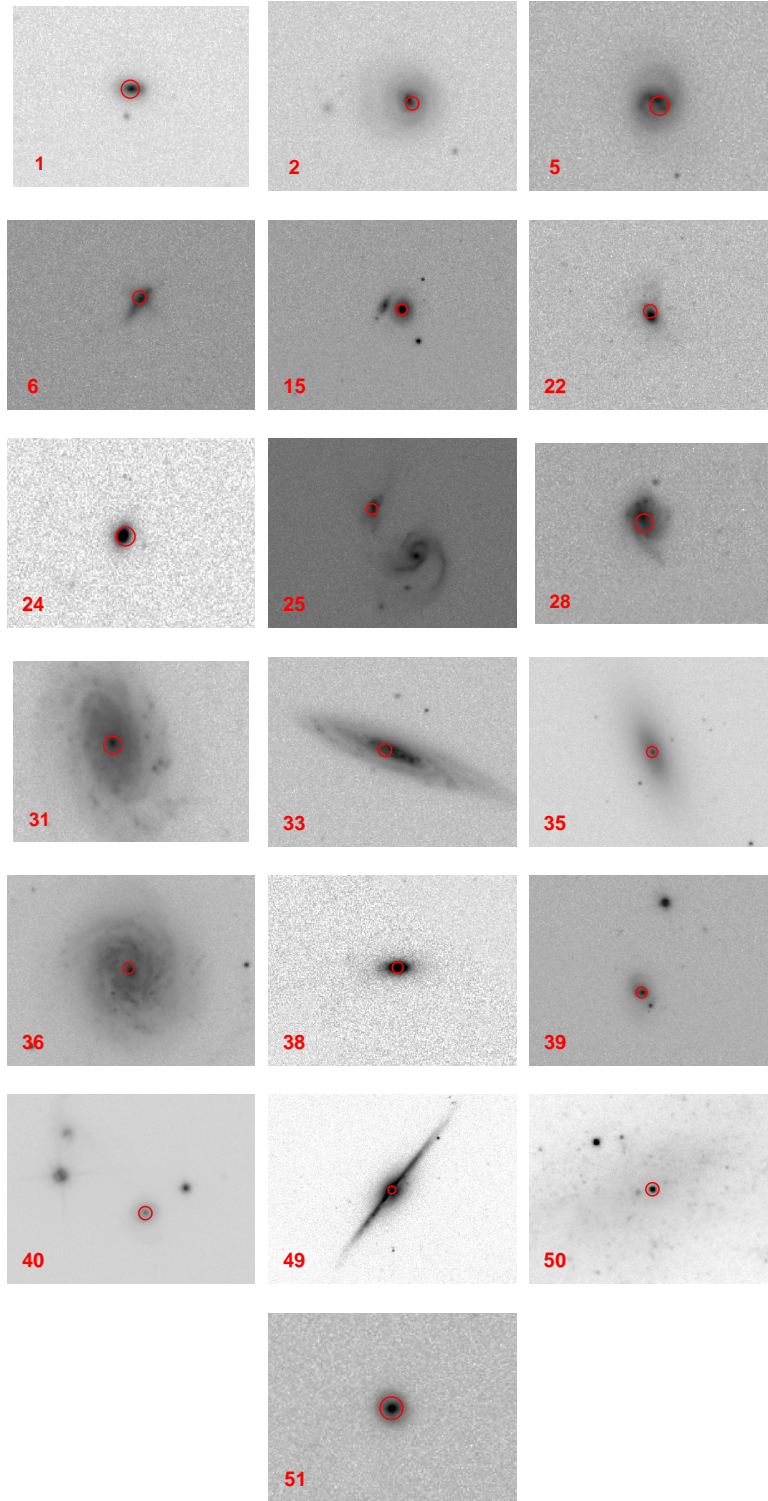


Fig. 1.— SDSS images in the r band of the sub-sample of our GiX catalogue showing evidence of nuclear sources emitting in X -ray and radio. The red circle (having a radius of $3''$) represents the position of the central candidate black hole and is positioned on the associated X -ray source coordinates.

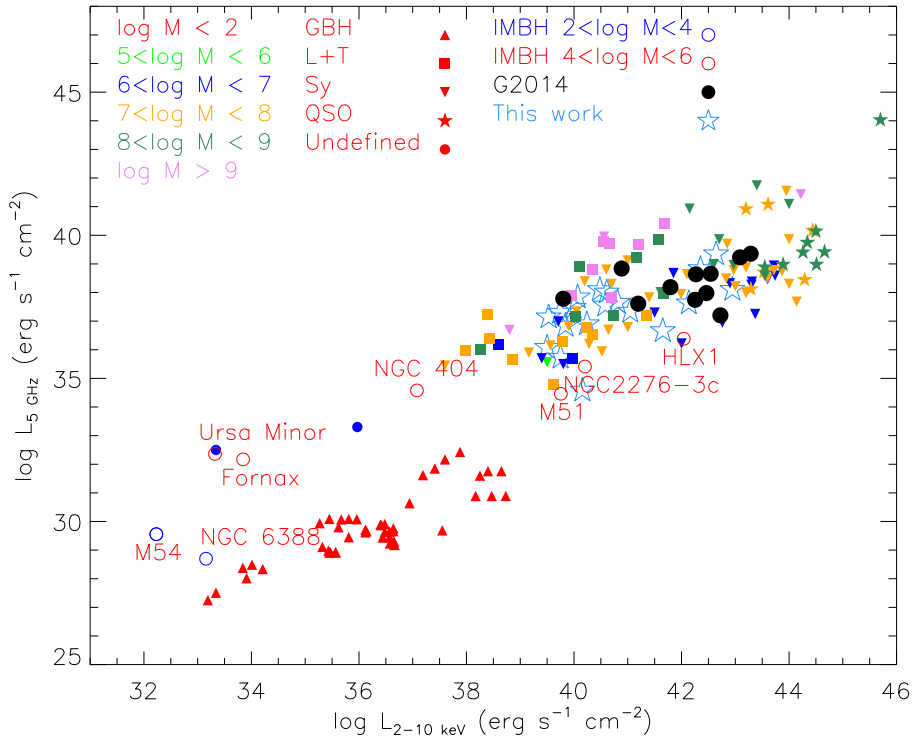


Fig. 2.— The fundamental plane adapted from Merloni et al. (2003) super-imposing also our results (dodger blue empty stars). We also consider Galactic BHs (GBH), Liners-Transition and quasi stellar objects (L-T and QSO, respectively), Seyfert nuclei (Sy), undefined sources, as well as IMBH candidates (open circles), already known in literature (see text for details). Filled black circles represent eleven low-mass AGN showing evidence of IMBHs with mass less than $10^{6.3} M_{\odot}$ (Gültekin et al. 2014).

scope Array) will be fully operational on-board the Russian Spektrum-Roentgen-Gamma (SRG) mission (see Merloni et al. 2012). This instrument will have a spatial resolution on axis comparable to that of the *XMM-Newton* satellite but with larger effective area. After the completion of the four year all-sky survey, an average exposure of 2548 s per FOV (0.83 deg^2) will allow one to detect rather faint objects with flux limits of $\sim 10^{-14} \text{ erg s}^{-1} \text{ cm}^{-2}$ and $\sim 10^{-13} \text{ erg s}^{-1} \text{ cm}^{-2}$ in the energy bands 0.5 – 2 keV and 2 – 10 keV, respectively. Hence, the combination of the two missions could result in the discovery of a remarkably high number of X-ray sources in low-mass galaxies up to moderate large redshifts. Further dedicated radio observations towards the selected targets will then permit to investigate the massive black hole properties in such galaxies. Indeed, as noted by Mezcua et al. (2016), determining the fraction of black holes in low-mass galaxies and the galaxy properties (as stellar density and star formation rate) at different redshifts could allow one to understand whether massive black holes form from a first generation of $\approx 100 M_{\odot}$ stellar seeds or from the growing of less massive black holes (with $\approx 10^4 - 10^6 M_{\odot}$) originated by the direct collapse of gas clouds in primordial halos (see, e.g. Pacucci et al. 2016).

If massive black holes are really so common in low-mass galaxies and ultra-compact dwarfs, this would have implications for the demographics of such objects. Based on their results about M60-UCD1, Seth et al. (2014) point to the fact that the amount of massive black hole in the Universe must be much larger than commonly thought. Of course, at least for sources #1 (NGC 1303) which shows a galaxy to black hole mass ratio very extreme, further follow-up observations both in X-rays and radio bands, as well as in the optical, are necessary in order to confirm (or reject) our results.

Acknowledgements

This research has made use of data obtained from the 3XMM *XMM-Newton* serendipitous source catalogue compiled by the 10 institutes of the *XMM-Newton* Survey Science Centre selected by ESA. We acknowledge the support by the INFN projects TASP (Theoretical Astroparticle Physics Project) and EUCLID. We thank the anonymous Referee for the suggestions that greatly improved the paper.

REFERENCES

- Amorisco, N. C., Evans, N. W., 2012, MNRAS, 419, 184A
- Bernardi, M., Sheth, R. K., Annis, J., et al., 2003, AJ, 125, 1817
- Blanton, M. R., & Roweis, S. 2007, AJ, 133, 734
- Cimatti, A., & Scaramella, R., 2012, Mem. S.A. it. Suppl., 19, 314
- Conroy, C. & Bullock, J.S., 2015, ApJ, 805, L2
- den Brok, M., Seth, A.C., Barth, A.J., et al., 2015, ApJ, 801, 16
- De Paolis, F., Ingrosso, G., Nucita, A. A., Qadir, A., & Zakharov, A. F., 2011, GReGr, 43, 977
- Earnshaw, H.M., 2016, AN, 337, 448
- Earnshaw, H.M., Roberts, T.P., Heil, L.M., et al., 2016, MNRAS, 456, 3840
- Evans, I. N., Primini, F. A., Glotfelty, K. J., et al., 2010, ApJS, 189, 37
- Gültekin, K., Cackett, E.M., King, A.L., Miller, J.M., Pinkney, J., 2014, ApJ, 788, L22
- Gyuk, K., Dalal, N., & Griest, N., 2000, in *Microlensing 2000, A New Era of Microlensing Astrophysics*, ASP Conference Series, Eds. Menzies J., & Sackett P. D., Vol. 239
- Falcke, H., Melia, F., & Agol, E., 2000, ApJL, 528, L13.
- Jansen, F., Lumb, D., Altieri, B., et al., 2001, A&A, 365, L1
- Kalberla, P.M.W., Burton, W. B., Hartmann, D., et al. 2005, A&A, 440, 775
- Kormendy, J., & Ho, L. C., 2013, ARA&A, 51, 511
- LaMassa, S. M., Yaqoob, T., Ptak, A. F., et al., 2014, ApJ, 787, 61
- Lemons, S. M., Reines, A. E., Plotkin, R. M., Gallo, E., Greene, J. E., 2015, ApJ, 805, 12L
- Maccarone, T. J., Kundu, A., Zepf, S. E., Piro, A. L., Bildsten, L., 2005b, MNRAS, 364, L61

- Magorrian, J., Tremaine, S., Richstone, D., 1998, *The Astronomical Journal*, 115, 2285
- Matti, G., 2002, *Phil. Trans. R. Soc. A*, 360., 2045
- Manni, L., Nucita, A.A., De Paolis, A., Testa, V., In-
grosso, G., 2015, *MNRAS*, 451, 2735
- Mateo, M., 1997, in *ASP Conf. Ser.*, 116, *The Nature
of Elliptical Galaxies*, Astron. Soc. Pac., San Fran-
cisco, (Eds., Arnaboldi M. et al.)
- Martin, N. F., de Jong, J. T. A., Rix, H.-W., 2008, *ApJ*,
684, 1075
- McConnachie, A. W., 2012, *The Astronomical Jour-
nal*, 144, 4
- Laureijs, R., et al., 2011, arXiv:1110.3193
- Merloni, A., Heinz, S., Di Matteo, T., 2003, *MNRAS*,
345, 1057
- Merloni, A., Predehl, P., Becker, W., et al., 2012,
arXiv:1209.3114
- Mezcua, M., Roberts, T.P., Lobanov, A.P., Sutton,
A.D., 2015, 448, 1893
- Mezcua, M., Civano, F., Fabbiano, G., Miyaji, T.,
Marchesi, S., 2016, *ApJ*, 817, 20
- Natarajan, P. 2014, *GRGr*, 46, 1702
- Nyland, K., Marvil, J., Wrobel, J. M., Young, L.M.,
Zauderer, B. A., 2012, *ApJ*, 753, 103
- Nucita, A. A., De Paolis, F., Ingrassio, G., Qadir, A., &
Zakharov, A. F., 2007, *PASP*, 119, 349
- Nucita, A. A., De Paolis, F., Ingrassio, G., Carpano, S.,
Guainazzi, M., 2008, *A&A*, 478, 763
- Nucita, A. A., Manni, L., De Paolis, F., Vetrugno, D.,
Ingrassio, G., 2013a, *A&A*, 550, 18
- Nucita, A. A., De Paolis, F., Manni, L., Ingrassio, G.,
2013b, *New Astronomy*, 23, 107
- Padmanabhan, N., Seljak, U., Strauss, M. A., et al.,
2004, *New Astronomy*, 9, 329
- Pacucci, F., Ferrara, A., Grazian, A., et al., 2016, *MN-
RAS*, 459, 1432
- Pardo, K., Goulding, A. D., Greene, J. E., et al., 2016,
arXiv:1603.01622
- Refregier, A., Amara, A., Kitching, T. D., et al., 2010,
arXiv:1001.0061
- Reines, A. E., Greene, J. E., Geha, M., 2013, *ApJ*, 775,
116
- Reines, A. E., 2014, *Nature*, 513, 322
- Reines, A. E., & Volonteri, M., 2015, *ApJ*, 813, 82
- Ricarte, A., & Dexter, J., 2015, *MNRAS*, 446 1973
- Rosa-Gonzalez, D., Burgarella, D., Nandra, K., et al.,
2007, *MNRAS*, 379, 357
- Rosen, S.R., Webb, N. A., Watson, M. G., et al., 2016,
A&A, 590, A1
- Seth, A.C., van den Bosch, R., Mieske, S., et al., 2014,
Nature, 513, 398
- Swartz, D.A., Soria, R., & Tennant, A.F., 2008, *ApJ*,
684, 282
- Volonteri, M., 2010, *A&ARv*, 18, 279
- Volonteri, M., & Gnedin, N. Y. 2009, *ApJ*, 703, 2113
- Watson, M.G., Schröder, A. C., Fyfe, D., et al., 2009,
A&A, 493, 339
- Webb, N., Cseh, D., Lenc, E., et al., 2012, *Science*,
337, 554
- Woo, J., & Urry, C.M., 2002, *ApJ*, 579, 530
- Wrobel, J.M, Greene, J.E., & Ho, L.C., 2011, *AJ*, 142,
113
- XMM-Newton Users Handbook, 2015, Issue 2.13
(Eds. Ebrero J. et al.)
- XRPS User's Manual, 2008, Issue 2.6 (Eds. Ehle M. et
al.)
- Zakharov, A. F., De Paolis, F., Ingrassio, G., & Nucita,
A.A. 2012, *NewAR*, 56, 64